Rare Metal Materials and Engineering
Volume 50, Issue 11, November 2021
Available online at www.rmme.ac.cn

Science Press

Cite this article as: Li Weirong, Dan Yun, Huang Xianxiang, et al. Microstructure Evolution, Tensile Behavior, and Wear Properties of AZ91 Alloys with Different Sn Contents by Rheocasting[J]. Rare Metal Materials and Engineering, 2021, 50(11): 3879-3884.

ARTICLE

Microstructure Evolution, Tensile Behavior, and Wear Properties of AZ91 Alloys with Different Sn Contents by Rheocasting

Li Weirong[1,2], Dan Yun[1], Huang Xianxiang[1], Guan Renguo[3], Ren Haobo[1], Li Yangde[2], Sun Lijuan[2], Zhang Jin[3], Tie Di[1]

[1] Key Laboratory of Lightweight Structural Materials Liaoning Province, Northeastern University, Shenyang 110819, China; [2] Dongguan Eontec Co., Ltd, Dongguan 523662, China; [3] Engineering Research Center of Continuous Extrusion, Ministry of Education, Dalian Jiaotong University, Dalian 116028, China

Abstract: The effect of different Sn contents on microstructure evolution, tensile behavior, and wear properties of AZ91 alloys by rheocasting was studied. The results show that the presence of Sn changes the solid solubility of Al in Mg matrix and effectively refines the microstructure of alloy matrix. The average grain size is refined from 105.0 μm to 42.1 μm after addition of 0.8wt% Sn. The heterogeneous precipitate nuclei are formed by the intermetallics with high melting point, which effectively refines the magnesium matrix during the rheo-solidification. These dispersed second phases suppress the formation of dendrites, further improving the mechanical properties. With increasing the Sn content, the wear rate of alloys is obviously decreased and the abrasive wear disappears gradually. The rheocast AZ91 alloy with addition of 3.0wt% Sn has the highest tensile strength and the best wear resistance.

Key words: AZ91 alloy; Sn; microstructure; tensile behavior; wear

As one of the lightest metallic materials, magnesium and its alloys have been widely applied in industry. Due to their high specific strength, low density, good recyclability, and good rigidity, they are highly valued by scientific researchers[1,2]. AZ91 alloy is one of the most widely used die-casting magnesium alloys, which is characterized by lightweight, high specific strength, good combination of castability and corrosion resistance, and good surface quality[3,4]. However, the ductility of AZ91 alloy is lower than that of traditional metallic materials, which restricts its applications[5-7]. The $Mg_{17}Al_{12}$ phases can form continuous network and be distributed along the grain boundaries, leading to the low ductility. Therefore, many researchers aim to improve the microstructural stability of AZ91 alloy by alloying which can effectively inhibit the generation of $Mg_{17}Al_{12}$ network. Alloying elements including calcium and rare earths can consume the aluminum atoms in the matrix and form aluminum-containing intermetallic compounds with high melting points, thereby reducing the formation of $Mg_{17}Al_{12}$ phases[8,9].

Previous studies reported that the appropriate amount of Sn can evidently refine the magnesium matrix, because the Mg_2Sn phase is precipitated preferentially when AZ91-Sn alloy solidifies due to the good ductility of Sn at normal temperature[10]. The melting point of β-$Mg_{17}Al_{12}$ phases in the magnesium matrix is lower than that of Mg_2Sn phases[11]. Consequently, the morphology distribution of Al-Mg phase is affected by the preferential precipitation of the Mg_2Sn phase. In previous studies[10], the microstructure and mechanical properties of AZ91 alloy with low Sn content (0.8wt% ~ 2.4wt%) were investigated. Therefore, the influence of different Sn contents on the solidification process, microstructure evolution, tensile behavior, and wear resistance of rheocast AZ91 alloys were further investigated in this research.

Received date: November 03, 2020
Foundation item: National Natural Science Foundation of China (51771045, U1764254); Fundamental Research Funds for the Central Universities (N2002016)
Corresponding author: Tie Di, Ph. D., Associate Professor, Key Laboratory of Lightweight Structural Materials Liaoning Province, School of Materials Science and Engineering, Northeastern University, Shenyang 110819, P. R. China, Tel: 0086-24-83681990, E-mail: tie-di@hotmail.com

Copyright © 2021, Northwest Institute for Nonferrous Metal Research. Published by Science Press. All rights reserved.

1 Experiment

The AZ91 alloys for investigation contained 0.0wt%, 0.4wt%, 0.8wt%, 1.2wt%, 2.4wt%, and 3.6wt% Sn, which were named as AZ91-*x*Sn with *x*=0, 0.4, 0.8, 1.2, 2.4, 3.6, respectively in this research. An inductively coupled plasma optical emission spectrometer (VARIAN, USA) was employed to analyze the chemical composition of the alloy. The materials were melted in an electrical furnace (Hengli, China) under protective atmosphere[12]. Before casting, the crucible, slag scoop, and the pressing cover were coated with the TiO_2/C_2H_5OH mold release of 0.5 mm in thickness. A rheological slurring machine equipped with an electromagnetic vibrator was used for the semi-solid rheocasting, as shown in Fig. 1[13,14]. The casting temperature was 680~690 °C, which is within the semi-solid temperature range of AZ91 alloy. The casting speed was 0.052 m/s and the vibration frequency was 100 Hz.

The metallographic structure was observed using an optical microscope (OM, DSX 500, Olympus, Japan). The phases in the alloy matrix were qualitatively analyzed by an X-ray diffractometer (XRD, PANalytical, Almelo, Netherlands). The microstructures were analyzed by X'Pert Highscore software. The microstructure and precipitate morphologies of the alloy were observed using the scanning electron microscope (SEM, JCM-5000, Nikon, Japan). The element distribution was determined and analyzed by an energy dispersive spectroscopy (EDS, Ametek, USA) coupled with SEM. The beam-milled specimens were further observed using high resolution transmission electron microscopy (HRTEM, JEM-2010, Japan) for phase identification. The fracture morphologies were observed by SEM and EDS. A friction tester (Spai, China) was used for the dry sliding wear tests. A spherical counterpart made from bearing steel (HBN 700) was used for the wear tests at the speed of 1.00 $m \cdot s^{-1}$. The total sliding distance was 2000 m and the applied load was 50 N. Mechanical polishing, ultrasonic cleaning, and vacuum drying processes were performed on the specimens before wear tests to assure the clean and smooth surfaces. The wear rate (WR) was calculated through the formula $WR=\Delta m/m_0$, where Δm is the mass difference of the specimen before and after the wear test, and m_0 is the initial mass before wear test.

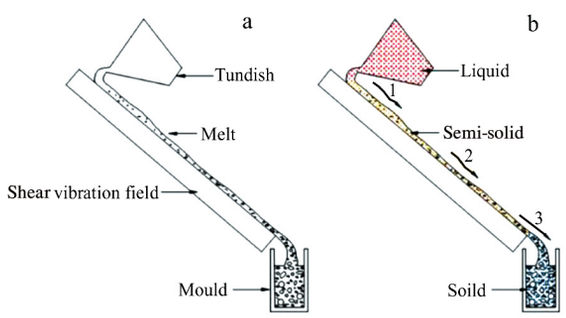

Fig.1 Schematic diagrams of rheocasting device with sheer vibration field (a) and melt flowing model (b)

2 Results and Discussion

The measured Sn contents of the AZ91-*x*Sn alloys with *x*= 0.4, 0.8, 1.2, 2.4, 3.6 are 0.43wt% ±0.01wt%, 0.82wt% ± 0.01wt%, 1.21wt% ±0.01wt%, 2.42wt% ±0.02wt%, and 3.63wt%±0.01wt%, respectively. The microstructures of the rheocast alloys, as shown in Fig. 2, mainly consist of gray α-Mg matrix and β-$Mg_{17}Al_{12}$ phase precipitated at grain boundaries in a semi-continuous form[15]. When the melt temperature drops below the liquid line, Sn and Al elements are concentrated at the solid-liquid interface in α-Mg matrix.

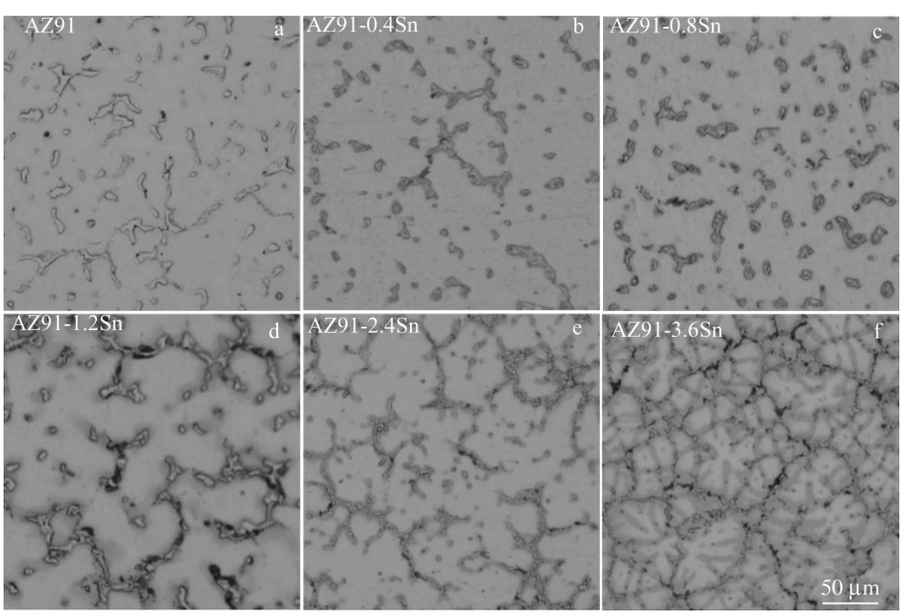

Fig.2 OM microstructures of AZ91-*x*Sn alloys: (a) *x*=0, (b) *x*=0.4, (c) *x*=0.8, (d) *x*=1.2, (e) *x*=2.4, and (f) *x*=3.6

With decreasing the temperature to the eutectic temperature (561 °C) of Mg-Sn alloys, the eutectic reaction of liquid phase →Mg+Mg_2Sn occurs in the remaining liquid phase. As Mg_2Sn phase is continuously generated, the content of surrounding Al is increased. The eutectic reaction of liquid phase→Mg+$Mg_{17}Al_{12}$ occurs when the temperature continues to drop to the eutectic temperature of the Mg-Al matrix. During the solidification process, the remaining liquid phase is transformed into eutectic Mg-Al-Sn alloys with decreasing the temperature, resulting in the ternary eutectic reaction of liquid phase→Mg+Mg_2Sn+$Mg_{17}Al_{12}$.

Fig.3 shows that most of the second phases are distributed along the grain boundaries in the matrix, and the rest second phases are distributed inside the grains. The white continuous phase is the $Mg_{17}Al_{12}$ eutectic phase, while the black phase on the surrounding contour is the precipitated β_{II}-$Mg_{17}Al_{12}$ phase containing 61.2at% Mg and 38.1at% Al, which is determined by EDS results. Mg_2Sn particles (69.3at% Mg and 27.2at% Sn) can be found inside the $Mg_{17}Al_{12}$ eutectic phases. It can be concluded from the SEM and EDS analyses that both the small-sized Mg_2Sn precipitates and the coarse $Mg_{17}Al_{12}$ precipitates are formed during the rheocasting process. The solidification process of the alloy is a non-equilibrium solidification in the actual rheocasting process and the average composition of the solid phase deviates from that of the equilibrium solidification. With decreasing the temperature, the composition of liquid phase becomes similar to that of eutectic. Therefore, the eutectic reaction occurs and the eutectic structure is formed. The α-Mg phase is formed faster than the eutectic due to existing pre-eutectic structures (α-Mg phase). Therefore, the second phases composed of $Mg_{17}Al_{12}$ and Mg_2Sn can only be found at grain boundaries. Compared with those of AZ91 alloy, the grain size and morphological distribution of second phases of alloys are changed by the addition of Sn (Fig. 2). After addition of Sn element, the microstructure of AZ91 alloy is refined and the second phases become shorter and denser. When the Sn content is less than 1.2wt%, the $Mg_{17}Al_{12}$ phase changes from reticular continuity to discontinuity (Fig. 2d). This phenomenon is particularly evident when the Sn content decreases to 0.8wt% . The $Mg_{17}Al_{12}$ phase of a short rod shape is completely and uniformly distributed in the matrix. When the Sn content increases from 1.2wt% to 3.6wt% , the second phases are distributed at the grain boundaries.

It can be concluded from the XRD patterns in Fig.4 that the rheocast AZ91 alloy is mainly composed of α-Mg matrix, $Mg_{17}Al_{12}$, and Mg_2Sn phases. With further addition of Sn, the diffraction peak intensity of Mg_2Sn phase becomes stronger, indicating an increase in Mg_2Sn content in the matrix. Aluminum is primarily distributed along the grain boundaries. A small number of the aluminum atoms are dissolved in the magnesium matrix, while the majority form the binary intermetallic compounds by reacting with magnesium atoms. The existence of Mg_2Sn inside the grain impedes the dislocation movement during deformation[16]. Fig. 5 shows HRTEM image of the dispersed second phases and the corresponding selected area electron diffraction (SAED) pattern. Mg_2Sn is predominantly dispersed inside the alloy matrix with an average diameter of about 10 nm, and its SAED pattern is indexed as the metastable phases with body-centered cubic (bcc) structure[10]. According to XRD and HRTEM analyses, the heterogeneous precipitate nuclei are formed by the intermetallics with high melting point, which effectively refines the magnesium matrix during the rheo-solidification. Compared with the case in AZ91 alloy without Sn addition, the second phases are also refined, and the Mg matrix is distributed homogeneously in the AZ91-*x*Sn alloys.

Fig.6 summaries the grain size and the tensile properties of the rheocast AZ91-Sn alloys. The average grain size of the AZ91 alloy is 105.0±2.3 μm. With increasing the Sn content, the average grain size is significantly decreased. The smallest average grain size of 42.1±1.5 μm can be found in AZ91-0.8Sn

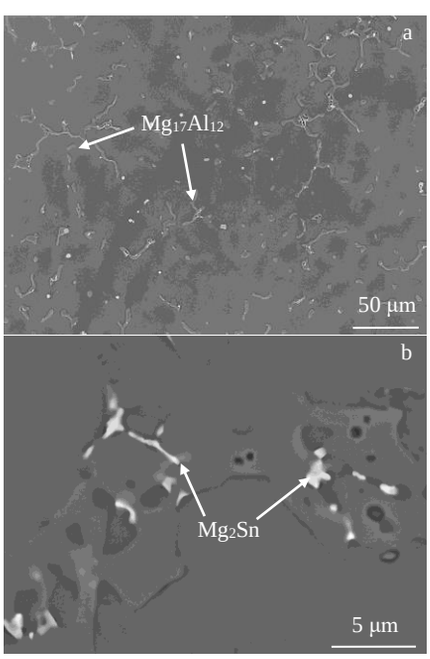

Fig.3 SEM images of coarse $Mg_{17}Al_{12}$ (a) and small-sized Mg_2Sn (b) precipitates in rheocast AZ91-3.6Sn alloy

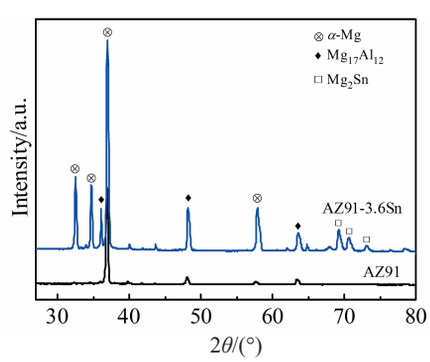

Fig.4 XRD patterns of rheocast AZ91 and AZ91-3.6Sn alloys

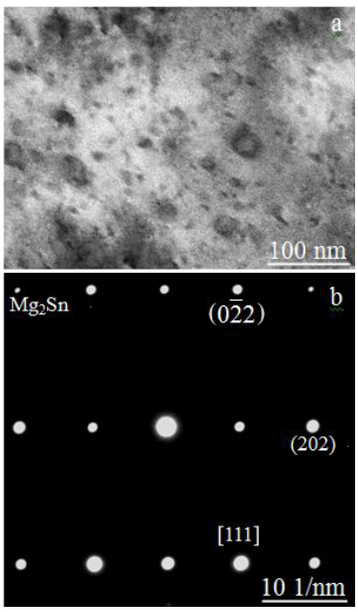

Fig.5 HRTEM image of AZ91-3.6Sn alloy (a) and SAED pattern of Mg_2Sn phase (b)

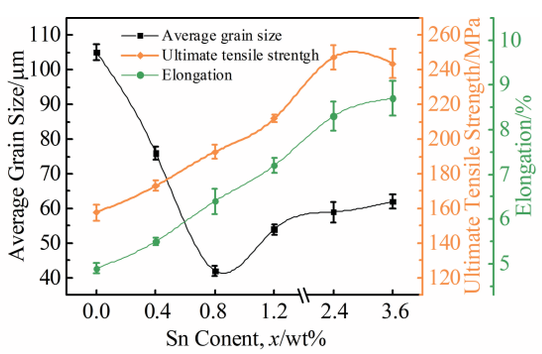

Fig.6 Average grain size, ultimate tensile strength, and elongation of AZ91-*x*Sn (*x*=0.0, 0.4, 0.8, 1.2, 2.4, 3.6) alloys

alloy. This significant grain refinement leads to the grain refinement strengthening effect. Therefore, both the tensile strength and the elongation of the alloys are improved. Compared with that of pure AZ91 alloy (157.7 MPa), the ultimate tensile strength of AZ91-2.4Sn alloy (247.2 MPa) increases by 57%. Due to the refined matrix, the high density grain boundaries can bear more stress[10,17]. Besides, the dispersed second phases suppress the formation of dendrites. Therefore, the refined non-dendritic microstructure can be observed in AZ91-Sn alloys (Fig.2), resulting in the improved mechanical properties. It is also notable that the addition of 3.6wt% Sn leads to a decrease in tensile strength whilst an increase in the elongation, because of the grain boundary sliding caused by the increasing amount of Mg_2Sn phases. Although these intermetallics can improve the tensile strength, the weaker bonding energy between the grains and the intermetallics causes stress sliding at the interfaces[18]. Therefore, the AZ91-3.6Sn alloy has the highest elongation and a relatively low tensile strength[19].

To study the fracture behavior of AZ91-*x*Sn (*x*=0.0, 0.4, 0.8, 1.2, 2.4, 3.6) alloys, SEM fractographs of tensile specimens were analyzed, as shown in Fig.7. Twin boundary fracture can be observed in all specimens[20]. Due to the low deformation absorbed energy, the fracture morphology of AZ91 alloy is primarily composed of river patterns and cleavage planes. Based on the cleavage steps and tearing edges of high density in the river patterns, it can be concluded that the cleavage fracture is the primary fracture type in AZ91 alloy. With increasing the Sn content, denser and deeper dimples can be observed in the AZ91-Sn alloys, indicating that the alloys undergo ductile fracture. Therefore, the AZ91-Sn alloys display ductile fracture morphologies, according to the presence of less quasi-cleavage planes and more dimples and tear ridges[21]. The worn surface of AZ91 alloy presents spalling areas (Fig. 8a). With increasing the Sn content, the worn surface is primarily composed of furrows and abrasive wear disappears. The wear rate of the AZ91-3.6Sn alloy is approximate 53% lower than that of the AZ91 alloy (Fig. 8c). It can be concluded that Sn alloying significantly improves the wear resistance of AZ91-Sn alloy.

At the beginning of the cooling process of alloy melt, the α-Mg matrix firstly solidifies. Due to the unbalanced solidification crystallization, when the temperature drops to the eutectic temperature, the eutectic reaction occurs in the residual liquid phases. The precipitates of reticular shape along grain boundaries form the divorced eutectic phases. When the Sn content is 0.8wt%, the second phases in the matrix are homogeneously distributed. The phases begin to show discontinuous morphology with increasing the Sn content. The solid solubility of Sn in magnesium matrix drops rapidly from 14.85wt% to 0.45wt% with decreasing the

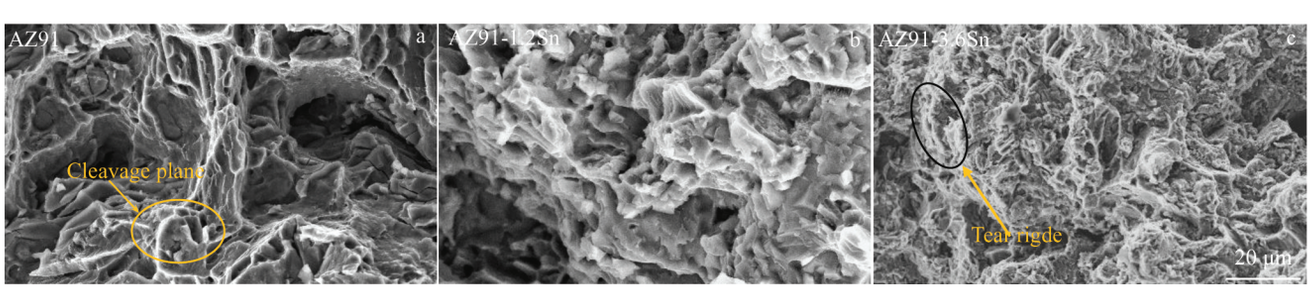

Fig.7 SEM fractographs of AZ91 (a), AZ91-1.2Sn (b), and AZ91-3.6Sn (c) alloys

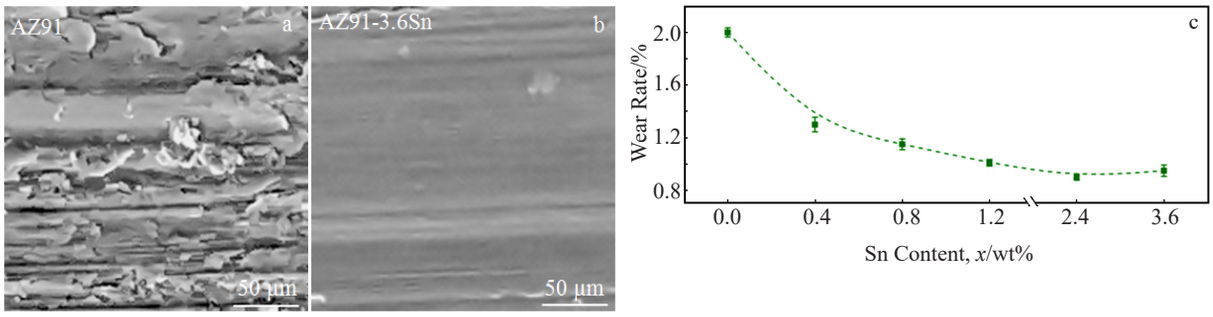

Fig.8 SEM images of worn surfaces of AZ91 (a) and AZ91-3.6Sn (b) alloys after dry sliding wear tests; wear rate of AZ91-*x*Sn (*x*=0.0, 0.4, 0.8, 1.2, 2.4, 3.6) alloys (c)

temperature from 561 °C to 200 °C[22]. Therefore, an enrichment of Sn atoms at the interfaces between solid phases and liquid phases can be observed.

$Mg_{17}Al_{12}$ has face-centered cubic (fcc) structure whilst Mg_2Sn has bcc structure. SEM images in Fig. 3 show the Mg_2Sn phase precipitated along with $Mg_{17}Al_{12}$ phases, indicating that $Mg_{17}Al_{12}$ is nucleated around the heterogeneous points composed of Mg_2Sn particles. As a result, the nucleation rate of $Mg_{17}Al_{12}$ is increased and accelerated with increasing the Sn content. Jo et al[23] reported the existence of the habit planes between $Mg_{17}Al_{12}$ and Mg_2Sn phases. The presence of (220)// (330) habit planes between Mg_2Sn and $Mg_{17}Al_{12}$ second phases is the primary reason why Mg_2Sn becomes the heterogeneous nucleation points[24]. In this case, the solidified α-Mg matrix firstly appears in the rheo-solidification process of AZ91-Sn alloys. With decreasing the temperature, the significant loss of Sn content in the alloy matrix leads to the enrichment of Sn element at the front-end interfaces of the liquid-solid. Therefore, the Mg_2Sn is precipitated according to the eutectic reaction of liquid phase→α-Mg+Mg_2Sn. As the solidification process proceeds, $Mg_{17}Al_{12}$ is precipitated and grows on the solid-liquid interface along the (220) surface of Mg_2Sn until the liquid phases entirely solidify[25]. The schematic diagram of the alloy solidification behavior is shown in Fig. 9. Due to the refined non-dendritic microstructure caused by rheo-solidification, the tensile strength and wear resistance are significantly improved.

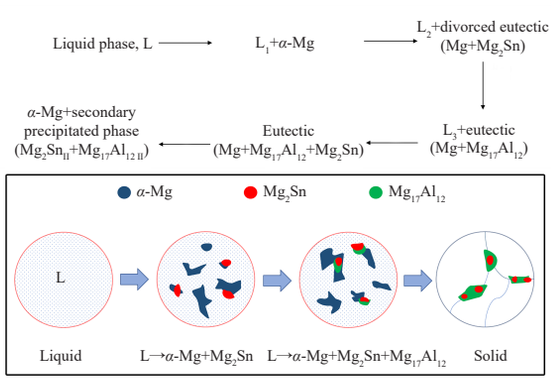

Fig.9 Schematic diagram of solidification behavior of AZ91-Sn alloys

3 Conclusions

1) The addition of Sn can refine the grain size of AZ91 alloys and modify the morphology of the β-$Mg_{17}Al_{12}$ phase during rheocasting process. Sn alloying is an effective method to refine both the alloy matrix and the precipitates.

2) Due to the grain refinement strengthening and the absence of dendrites, both the tensile strength and the elongation are improved. With increasing the Sn content, the average grain size is significantly decreased, resulting in the evident grain refinement strengthening effect. Compared with that of pure AZ91 alloy, the ultimate tensile strength of AZ91-2.4Sn alloy increases by about 57%.

3) The wear resistance of the AZ91 alloy is improved after Sn alloying, and the wear mechanism changes from spalling wear to furrow wear.

References

1 Lamm S, Matschkal D, Göken M *et al*. *Materials Science and Engineering A*[J], 2019, 761: 137 964
2 Peng Qiuming, Sun Yong, Ge Bingcheng *et al*. *Acta Materialia* [J], 2019, 169: 36
3 Pan Fusheng, Yang Mingbo, Chen Xianhua. *Journal of Materials Science and Technology*[J], 2016, 32(12): 1211
4 Du Wenwen, Sun Yangshan, Min Xuegang *et al*. *Materials Science and Engineering A*[J], 2003, 356(1-2): 1
5 Chalasani D, Jain M K, Shankar S *et al*. *Journal of Materials Engineering and Performance*[J], 2018, 28(1): 123
6 Tie Di, Guan Renguo, Liu Huinan *et al*. *Acta Biomaterialia*[J], 2016, 29: 455
7 Fu H, Ge B C, Xin Y C *et al*. *Nano Letters*[J], 2017, 17(10): 6117
8 Fu Li, Wang Xibo, Gou Peili *et al*. *Advanced Engineering Materials*[J], 2017, 19(12): 1 700 230
9 Cai Huisheng, Guo Feng, Su Juan *et al*. *Physica Status Solidi B* [J], 2019, 257(5): 1 900 453
10 Tie D, Zhang B Y, Yan L F *et al*. *Crystals*[J], 2019, 9(12): 641
11 Kim B H, Lee S W, Park Y H *et al*. *Journal of Alloys and Compounds*[J], 2010, 493(1-2): 502

12 Kim J K, Oh S H, Kim K C *et al*. *Materials Transactions*[J], 2017, 58(6): 963
13 Guan Renguo, Zhao Zhanyong, Chao Runze *et al*. *Metals Materials International*[J], 2013, 19(5): 949
14 Parizi M T, Habibolahzadeh A, Ebrahimi G R. *Materials Science and Engineering A*[J], 2017, 693: 33
15 Feng Hui, Liu Shuhong, Du Yong *et al*. *Journal of Alloys and Compounds*[J], 2017, 695: 2330
16 Radha R, Sreekanth D. *Journal of Magnesium and Alloys*[J], 2020, 8(2): 452
17 Dai Shuai, Bian Zeyu, Wu Wenbo *et al*. *Materials Science and Engineering A*[J], 2020, 792: 139 838
18 Wu K C, Chang S Y, Yeh J W. *Materials Science and Engineering A*[J], 2015, 646: 201
19 Wang Xiaoyuan, Wang Yufei, Wang Cheng *et al*. *Journal of Materials Science and Technology*[J], 2020, 49: 117
20 Liu Feiya, Xin Renlong, Zhang Mingxing *et al*. *Acta Materialia* [J], 2020, 195: 263
21 Yu Zhaochen, Huang Qianfei, Zhang Wentao *et al*. *Materials Research Express*[J], 2020, 7(7): 76 505
22 Wang Bo, Chen Xianhua, Pan Fusheng *et al*. *Progress in Natural Science: Materials International*[J], 2017, 27(6): 695
23 Jo S M, Kim S D, Kim T H *et al*. *Journal of Alloys and Compounds*[J], 2018, 749: 794
24 Elsayed F R, Sasaki T T, Mendis C L *et al*. *Materials Science and Engineering A*[J], 2013, 566: 22
25 Kim B, Do J, Lee S *et al*. *Materials Science and Engineering A* [J], 2010, 527(24-25): 6745

流变铸造AZ91-Sn合金的组织演化、拉伸行为及磨损性能

李卫荣[1,2]，但　昀[1]，黄显祥[1]，管仁国[3]，任浩博[1]，李扬德[2]，孙丽娟[2]，张　晋[3]，铁　镝[1]
(1. 东北大学 辽宁省轻量化用关键金属结构材料重点实验室，辽宁 沈阳 110819)
(2. 东莞宜安科技股份有限公司，广东 东莞 523662)
(3. 大连交通大学 连续挤压教育部工程研究中心，辽宁 大连 116028)

摘　要：研究了不同Sn含量流变铸造AZ91合金的组织演化、拉伸行为及磨损性能。结果表明：Sn的合金化改变了Al在镁基体中的固溶度，并且显著细化了微观组织。加入0.8%（质量分数，下同）的Sn后，合金平均晶粒尺寸从105.0 μm降至42.1 μm。高熔点的金属间化合物为析出相提供了异质形核点，这些弥散析出的第二相在流变凝固过程中有效地细化了镁基体。弥散分布的第二相抑制了枝晶组织生长，从而进一步提升了合金的力学性能。随着Sn含量的增加，合金磨损率显著降低，磨粒磨损逐渐消失。3.0%Sn合金化的流变铸造AZ91合金具有最高的抗拉伸强度以及最好的耐磨损性能。

关键词：AZ91合金；Sn；微观组织；拉伸行为；磨损

作者简介：李卫荣，男，1974年生，工程师，东莞宜安科技股份有限公司，广东 东莞 523662，电话：0769-23076998，E-mail：liwr@e-ande.com